Available online at www.sciencedirect.com
SCIENCE DIRECT
Journal of Magnetic Resonance 179 (2006) 280–289
JMR Journal of Magnetic Resonance
www.elsevier.com/locate/jmr

Communication

Sensitivity quantification of remote detection NMR and MRI

J. Granwehr *,[1], J.A. Seeley [2]

Materials Sciences Division, Lawrence Berkeley National Laboratory, Department of Chemistry, University of California, Berkeley, CA 94720, USA

Received 25 October 2005; revised 16 December 2005
Available online 18 January 2006

Abstract

A sensitivity analysis is presented of the remote detection NMR technique, which facilitates the spatial separation of encoding and detection of spin magnetization. Three different cases are considered: remote detection of a transient signal that must be encoded point-by-point like a free induction decay, remote detection of an experiment where the transient dimension is reduced to one data point like phase encoding in an imaging experiment, and time-of-flight (TOF) flow visualization. For all cases, the sensitivity enhancement is proportional to the relative sensitivity between the remote detector and the circuit that is used for encoding. It is shown for the case of an encoded transient signal that the sensitivity does not scale unfavorably with the number of encoded points compared to direct detection. Remote enhancement scales as the square root of the ratio of corresponding relaxation times in the two detection environments. Thus, remote detection especially increases the sensitivity of imaging experiments of porous materials with large susceptibility gradients, which cause a rapid dephasing of transverse spin magnetization. Finally, TOF remote detection, in which the detection volume is smaller than the encoded fluid volume, allows partial images corresponding to different time intervals between encoding and detection to be recorded. These partial images, which contain information about the fluid displacement, can be recorded, in an ideal case, with the same sensitivity as the full image detected in a single step with a larger coil.

Keywords: NMR; MRI; Remote detection; Sensitivity; Indirect detection; Flow

1. Introduction

NMR remote detection, a novel technique to spatially and temporally separate encoding and detection of nuclear spin magnetization, has the potential to enhance the sensitivity of NMR spectroscopy and imaging experiments. It employs a flowing sensor medium that samples a stationary analyte of interest, which can be a liquid, a surface, a porous medium, or void space [1,2]. In these experiments the sensor medium, thus far hyperpolarized ^{129}Xe [3], is first introduced to a sample of interest, is encoded with information regarding that sample, and is then transferred to a different location for sensitive detection. This separation of the encoding and detection steps allows optimizing them independently. The encoding region may be configured in the most convenient way to accommodate the sample, while different conditions optimized for sensitivity are used in the detection region. This article aims to provide a more quantitative discussion of the sensitivity achievable with this technique.

The longitudinal magnetization of the sensor medium is the property that is altered by the encoding step. An arbitrary pulse sequence can be used that is able to transfer the desired information about the stationary analyte onto longitudinal magnetization of the sensor medium. This information can be the chemical shift of the sensor medium in contact with the sample [1]. An experiment to encode a heteronuclear spectrum from the stationary analyte to the mobile sensor using long-range intermolecular dipole–dipole interactions was suggested as well [4]. Void-space imaging experiments have been performed with phase-encoding

* Corresponding author. Fax: +1 510 486 5744.
E-mail address: joga@waugh.cchem.berkeley.edu (J. Granwehr).
[1] Present address: Sir Peter Mansfield Magnetic Resonance Centre, University of Nottingham, Nottingham NG7 2RD, UK.
[2] Present address: MIT Lincoln Laboratory, 244 Wood St., Lexington, MA 02420, USA.

1090-7807/$ - see front matter © 2005 Elsevier Inc. All rights reserved.
doi:10.1016/j.jmr.2005.12.006

[2,5] as well as projection reconstruction [1]. In experiments that involve a transient evolution of transverse magnetization during encoding, one phase component after each evolution time t_1^r is stored with a 90° pulse as longitudinal magnetization, M_z, and at the same time any remaining M_z is transferred into the xy plane. Stored as polarization, the magnetization follows the external field adiabatically and is protected against dephasing due to field inhomogeneities [6], thus the sensor can flow through field gradients to the detector in a remote location without losing its information. This travel step is only restricted by the longitudinal relaxation of the sensor medium. The travel time, t_{trav}, has to be on the timescale of its longitudinal relaxation time T_1 or shorter, so at least part of the encoded magnetization survives. At the same time any coherent magnetization dephases, because the sensor usually experiences considerable field gradients while traveling between encoding and detection environments. Therefore this traveling step acts like a z filter. When the encoded sensor medium reaches the detector, its longitudinal magnetization is read out. In other words, the indirect dimension of the resulting data set provides the information about the encoding environment. Therefore, remote detection NMR is inherently a point-by-point technique.

Remote detection enables experiments at low magnetic fields without suffering the consequence of low sensitivity. This is relevant for the study of samples containing susceptibility gradients or electrically conducting components such as human subjects with metallic implants. These susceptibility gradients scale linearly with the applied magnetic field. Another example of a constraint imposed on the encoding environment is the size of the sample of study. Although a large coil may be needed to encode signal in a large object, a smaller coil can be used to detect extracted concentrated sensor [7].

A different experimental approach with remote detection is to record the arrival of the sensor medium in the detector transiently as a function of the encoded information in a time-of-flight (TOF) experiment [5,7]. While the optimum signal energy is obtained if all of the encoded sensor medium is collected and read out at once, this TOF detection provides additional information, as it allows one to correlate the TOF with the encoded information, for example by mapping the flow field of the fluid as it flows through the stationary analyte. If an inductive detector is used, such a flow profile can be measured by applying a train of 90° pulses in the remote coil and recording the amplitude of the FID after each pulse. This technique complements currently used flow imaging experiments, which measure local velocity vectors and not the global flow field [8,9].

Not only can the signal be measured by inductive detection, but any technique can be used that is capable of sensitively measuring the magnetization or the polarization of the sensor medium. For example, DC magnetometers such as superconducting quantum interference devices (SQUIDs) [10] or optical magnetometers [11] may be preferred at low fields. Alternatively, spin-exchange optical detection could serve as a technique that is specific to measure the polarization of noble gas sensor media. This technique is based on the transfer of spin-polarization from the noble gas to Rb electron spins [12]. In addition to using inductive detection with pulsed rf irradiation, it is also possible to use continuous-wave (cw) techniques. Since at least with hyperpolarized ^{129}Xe only one line with known position must be detected, this approach would not have the sensitivity disadvantage of a conventional cw experiment [13].

2. Theory

While in previous publications the detector was considered the main sensitivity determining parameter, the involved dephasing times influence the sensitivity as well. In general, the sensitivity of NMR remote detection can be analyzed with the same approach as a conventional two-dimensional (2D) NMR experiment [13,14], with the remote detection dimension corresponding to the direct dimension of the conventional experiment. This sensitivity discussion can be split into a detector-independent part that includes the timing of the experiment and the relevant dephasing and relaxation times, and a detector dependent part that discusses the ability of the different detectors to measure the polarization or the magnetic moment of the sensor spins. Note that sensitivity is not simply the signal-to-noise ratio (SNR), ψ, rather, it is the SNR per square root time, $\Psi = \psi/\sqrt{T_{tot}}$, where T_{tot} is the total duration of the experiment. This is the quantity that will be compared in the following discussion.

2.1. Remote detection of a transient signal

A possible pulse sequence for a spectroscopy experiment with remote detection is shown in Fig. 1. With direct detection, the complex signal induced in the encoding coil by the FID of a single resonance can be described as

$$s(t_d) = s^e(t_d)\exp(i\Omega t_d) \tag{1}$$

with the envelope function, $s^e(t_d)$, and the offset precessional frequency, Ω. In the following calculations, it is assumed that s^e represents an exponential decay with time constant T_2^d. The signal is sampled by M sampling points from time 0 to t_d^{max}, spaced by the dwell time Δt. Assuming white random noise limited by an analog filter with a bandwidth

$$\Delta f = \frac{1}{\Delta t} = \frac{M}{t_d^{max}} \tag{2}$$

that cuts off frequencies above the Nyquist frequency of the sampling process, the r.m.s. noise amplitude is

$$\sigma_d = \sqrt{\Delta f}\,\rho_d = \sqrt{\frac{M}{t_d^{max}}}\rho_d, \tag{3}$$

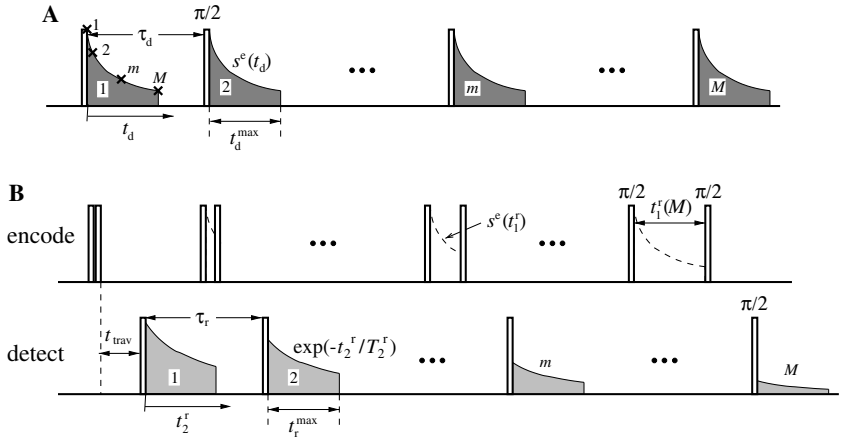

Fig. 1. Sensitivity comparison between direct (A) and remote detection (B). With direct detection, a complex FID is recorded transiently with M data points, which are marked with '×' symbols in the first FID. Remotely, $2M$ encoding steps are necessary to obtain the same data set, which allows one to perform $2M$ signal averaging steps in the direct dimension in the same time. The encoding and detection steps in the remote experiment are intermingled, therefore only a time overhead corresponding to one travel time occurs. The stored magnetization of the mth encoding step corresponds to the mth data point with direct detection and marks the magnetization at the beginning of the remote detection. The sensitivity is proportional to the total area under all the FIDs in both cases.

where ρ_d is the square root of the frequency-independent power spectral density and t_d^{max} is the total evolution time. Because M data points are recorded during the repetition time τ_d, we can say that the time it takes to acquire one data point is $t_d^{aq} = \tau_d/M$. Thus, with direct detection of a transient signal we get a sensitivity for one data point of

$$\Psi_d = \left|\frac{s(t_d)}{\sigma_d\sqrt{t_{aq}}}\right| = \frac{s^e(t_d)}{\rho_d}\sqrt{\frac{t_d^{max}}{\tau_d}}. \tag{4}$$

where t_d^{max}/τ_d represents the duty cycle of this experiment.

To determine the sensitivity of one point of a remotely detected FID, the signal is described by

$$s(t_1^r, t_2^r) = s^e(t_1^r)\left[\cos(\Omega t_1^r) + j\sin(\Omega t_1^r)\right]\exp\left(i\Omega_2 t_2^r - \frac{t_2^r}{T_2^r}\right), \tag{5}$$

where we assume that the travel time t_{trav} of the sensor medium is much shorter than its T_1. This signal oscillates at Ω_2 and decays with a time constant T_2^r during remote detection. t_2^r denotes the evolution time parameter in the remote detection dimension, t_1^r is the evolution time in the encoding dimension, and Ω represents the precessional frequency in the encoding environment. The imaginary units i and j are independent, equivalent to a hypercomplex encoding scheme [13]. The information encoded pointwise along t_1^r corresponds to the signal described by Eq. (1). Since only one phase component of the transverse magnetization can be stored at the end of each encoding period, the phase of the signal is lost between encoding and detection. Two encoding steps are necessary to map out one point of a complex FID, e.g., by applying the storage pulse along $-y$ and x in two subsequent encoding steps to encode $M_x(t_1^r)$ and $M_y(t_1^r)$, respectively.

To optimize the sensitivity of a spectrum, the time-domain signal may be multiplied with a weighting function $h(t)$. Because the remotely detected signal provides merely an amplitude value for each encoding step, it is reasonable to use a matched weighting function, $h_m(t_2^r) = \exp(-t_2^r/T_2^r)$, to maximize the sensitivity. The application of a matched filter results in a time constant $T_2^r/2$ of the signal. This filter will only be applied in the t_2^r dimension of the remote experiment for this treatment. Since it is not applied in the t_1^r dimension, the dimension analogous to the t_d dimension we are comparing it to, we do not need to apply a filter to the directly detected signal of Eq. (1) for a fair comparison. Each complex data point in the t_1^r dimension is recorded with a sensitivity

$$\begin{aligned}\Psi_r &= \left|\frac{S(t_1^r)}{\sigma_N\sqrt{t_r^{aq}}}\right|_{matched} \\ &= \frac{|s(t_1^r)|}{\rho_r}\sqrt{\left[\frac{t_r^{max}}{t_r^{aq}}\right]\left[\frac{1}{t_r^{max}}\int_0^{t_r^{max}}\left[\exp\left(-\frac{t_2^r}{T_2^r}\right)\right]^2 dt_r\right]} \\ &= \frac{s^e(t_1^r)}{\rho_r}\sqrt{\frac{T_2^r}{2(2\tau_r + t_{trav}/M)}\left(1-\exp\left(-\frac{2t_r^{max}}{T_2^r}\right)\right)},\end{aligned} \tag{6}$$

where $S(t_1^r)$ is the peak height σ_N the r.m.s. noise amplitude in the frequency domain of the remote dimension, t_r^{aq} is the time to acquire one data point, and τ_r is the repetition time of the experiment with remote detection. If encoding and detection are intermingled, the time for the fluid to flow from the encoding location to the detector, t_{trav}, contributes only once to the total experiment time, and $t_r^{aq} = 2\tau_r + t_{trav}/M$. For a typical number of data points M on the order of at least 100, we can neglect this additional contribution to the total experiment time, as $t_{trav}/M \ll \tau_r$. In Eqs. (4) and (6), the influence of longitudinal relaxation in the encoding environment and between the encoding and detection step in the case of remote detection was not considered. A factor ϱ is introduced in the following equations to account for this effect, which is discussed

later. The relative sensitivity between remote and direct detection can now be written as

$$\left[\frac{\Psi_r}{\Psi_d}\right]_{trans} = \frac{\Lambda\varrho}{\sqrt{2}}\sqrt{\left[\frac{T_2^r/2\tau_r}{t_d^{max}/\tau_d}\right]\left[1-\exp\left(-\frac{2t_r^{max}}{T_2^r}\right)\right]}, \quad (7)$$

where 'd' and 'r' denote the corresponding parameters of the direct and the remote experiment, respectively. Λ represents the relative SNR between remote detector and encoding circuit as obtained with an identical sample and equal experimental parameters. The factor $1/\sqrt{2}$ is a result of the fact that two cycles are required to obtain the complex signal with remote detection. The relaxation term is ideally $\varrho = 1$ if the longitudinal relaxation of the sensor fluid can be neglected, but it can be significantly lower for fluids relaxing fast on the time scale of an encode–detect cycle. Eq. (7) is not dependent on M; the sensitivity ratio of remote-to-direct detection is independent of the number of points in the spectrum even though adding more points increases the experimental time.

Remote detection can be considered to be an experiment in which the signal averaging is done in the direct dimension with a certain time constant, which is $T_2^r/2$ in this case. The interferogram is collected in the indirect dimension. In contrast, in an experiment with direct detection the interferogram is recorded transiently, and signal averaging to improve the SNR is done in an indirect dimension. Each trace has the same signal amplitude, and therefore the time constant, in analogy to that with remote detection, is infinitely long.

Depending on the value of T_2^r, Eq. (7) can be simplified. Assuming that $\varrho = 1$ and $\tau_d = \tau_r$, we get

$$\left[\frac{\Psi_r}{\Psi_d}\right]_{trans} \approx \frac{\Lambda}{\sqrt{2}}\sqrt{\frac{T_2^r}{2t_d^{max}}} \quad \text{if } t_r^{max} > T_2^r, \quad (8)$$

$$\left[\frac{\Psi_r}{\Psi_d}\right]_{trans} \approx \frac{\Lambda}{\sqrt{2}} \quad \text{if } t_r^{max} \ll T_2^r. \quad (9)$$

The first approximation is realistic in continuous flow experiments. Immediately after each detection pulse, the fluid starts to flow out of the detection volume, thus shortening T_2^r. The second approximation may be reasonable in stopped-flow mode in a well-shimmed detection environment. This is the ideal case where the sensitivity ratio depends, except for the factor $\sqrt{2}$, only on Λ.

2.2. Remote detection of a point-by-point experiment

The situation is different in an experiment where the transient dimension of the direct detection experiment itself measures only the amplitude and the phase as opposed to the time evolution of the signal, and the data set is recorded point-by-point. This is the case for example in an MRI experiment with phase encoding in all three dimensions. Here, the same number of encoding steps is necessary with direct and with remote detection, thus the sensitivity of the two modalities can be compared in a straightforward manner by determining the 1D sensitivity in both environments. Using the same formalism as for Eq. (7), this yields

$$\left[\frac{\Psi_r}{\Psi_d}\right]_{pp} = \frac{\Lambda\varrho}{\sqrt{2}}\sqrt{\left[\frac{t_r^{max}}{\tau_r}\right]\frac{\frac{1}{t_r^{max}}\int_0^{t_r^{max}}\left[\exp\left(-\frac{t_2^r}{T_2^r}\right)\right]^2 dt_2^r}{\frac{1}{t_d^{max}}\int_0^{t_d^{max}}\left[\exp\left(-\frac{t_d}{T_2^d}\right)\right]^2 dt_d}}$$

$$= \frac{\Lambda\varrho}{\sqrt{2}}\sqrt{\frac{\frac{T_2^r}{\tau_r}\left(1-\exp\left(-\frac{2t_r^{max}}{T_2^r}\right)\right)}{\frac{T_2^d}{\tau_d}\left(1-\exp\left(-\frac{2t_d^{max}}{T_2^d}\right)\right)}} \approx \frac{\Lambda}{\sqrt{2}}\sqrt{\frac{T_2^r}{T_2^d}}. \quad (10)$$

For the approximation it was assumed that $\varrho = 1$, $\tau_d = \tau_r$, and $t_r^{max} > T_2^r$, $t_d^{max} > T_2^d$. A comparison between Eqs. (7) and (10) shows that the potential signal advantage of remote detection in this second case is considerably larger than for transient experiments because the bandwidth of the direct experiment is determined by the signal decay time and not by the signal averaging. This is particularly important for samples with large susceptibility gradients, which cause fast dephasing of the directly detected transverse magnetization.

In the above calculations, it was assumed that all of the sensor medium gets fully regenerated between different repetitions of the experiment, which is reasonable because it is not a T_1 decay that determines this "relaxation," but a flow that forces the encoded sensor to move ahead. We have also neglected to account for the possibility that the sensor medium is dispersed between encoding and detection and is thereby diluted with unencoded fluid. This would require either a detector with a bigger active volume to assure that all the encoded fluid can be read out in one experiment, or multiple detection steps to catch all the encoded gas. In the case of a spectroscopy experiment without spatial dependence of the encoded information, it is not necessary to gather all the encoded fluid. However, the signal would be scaled proportionately to the amount of encoded fluid in the detector. If encoding steps are close enough to each other that a significant fraction of fluid gets encoded more than once, artifacts similar to those experienced with short repetition times in conventional 2D spectra can be expected [15]. If spatial information is encoded, it is required that the entire encoded sensor medium is detected. If it is diluted, the sensitivity is reduced, but the image can still be reconstructed accurately. However, if some of the encoded fluid remains undetected, the image will be weighted unevenly [2].

2.3. Influence of longitudinal relaxation during fluid flow

When the sensor medium flows from the encoding environment to the detector, it experiences two different environments, first the stationary sample in the encoding volume where its longitudinal relaxation time is T_1^d, and then the tubing that connects the encoding and the detection volume where its longitudinal relaxation time is T_1^r. In this latter environment, the relaxation of fluid simply causes the remote sensitivity to be multiplied by a factor

$\exp(-\tau_o/T_1^r)$, where τ_o is the time it takes the fluid from the outlet of the stationary analyte to reach the detector. This is close to unity for ^{129}Xe, but can be considerably smaller for a different sensor medium, especially for long distances between the encoding volume and the detector.

The longitudinal relaxation of the sensor medium inside the encoding environment has to be discussed separately for hyperpolarized media like ^{129}Xe and Boltzmann polarized spins. In the case of a hyperpolarized medium, we assume for simplicity that its equilibrium polarization is orders of magnitude lower and not detectable, therefore no background signal remains after complete relaxation towards equilibrium. The history of the polarized medium until it reaches the inlet of the stationary sample is not relevant, and we can consider the polarization at this inlet as the initial polarization of our experiment. In the case of direct detection, the signal then decays with T_1^d until the actual experiment takes place. Therefore, the signal at the inlet is stronger than the signal at the outlet. In case of an MRI experiment, the resulting image has to be weighted accordingly [16], and the SNR is spatially dependent. In a remote experiment, assuming the simple case of uniform flow distances through the stationary sample and low dispersion, all of the fluid remains inside the stationary sample approximately for constant time τ_i and relaxes uniformly towards a value corresponding to the lowest value in the experiment with direct detection, as for hyperpolarized fluids it does not matter whether relaxation happened prior or after the encoding step. Therefore, with remote detection no correction of the image for inhomogeneous initial spin polarization due to relaxation is necessary, but the relative sensitivity between remote and direct detection becomes spatially dependent. The result of Eq. (10) has to be scaled by a factor

$$\varrho_{mri}(\mathbf{r}) = \exp\left(-\frac{t_i(\mathbf{r})}{T_1^d} - \frac{\tau_o}{T_1^r}\right), \tag{11}$$

where $t_i(\mathbf{r})$ is the time it takes for the fluid to flow from location $\mathbf{r}$ inside the stationary sample the outlet. In the case of a spectroscopy experiment, the signal has to be averaged over the whole encoded volume for the direct experiment, while again for the remote experiment the polarization can be considered uniform. One obtains the scaling factor

$$\begin{aligned}\varrho_{nmr} &= \exp\left(-\frac{\tau_o}{T_1^r}\right)\frac{1}{\tau_i}\int_0^{\tau_i}\exp\left(-\frac{t_i}{T_1^d}\right)dt_i \\ &= \frac{T_1^d}{\tau_i}\left(1-\exp\left(-\frac{\tau_i}{T_1^d}\right)\right)\exp\left(-\frac{\tau_o}{T_1^r}\right)\end{aligned} \tag{12}$$

for experiments without spatial selectivity and if a cylindrical sample is assumed with a uniform fluid flow velocity, whereby it is not necessary to perform an integration over the whole encoding volume.

With Boltzmann polarized fluids, the situation is reversed. An experiment with direct detection has a uniform spin polarization across the whole sample, while with remote detection the signal relaxes back to its equilibrium value between the encoding step, at which point the magnetization is uniform across the sample, and the detection step. The signal from inside the stationary sample is inhomogeneously weighted with $\exp(-t_i(\mathbf{r})/T_1^d)$. Therefore, the same ϱ_{mri} as with hyperpolarized fluids is obtained. But this time, an image obtained with remote detection has to be corrected for inhomogeneous weighting of the signal due to relaxation. As long as dispersion in the tubing connecting the outlet of the sample with the detection volume is low, this correction is straightforward in a TOF experiment, where it is known how long the fluid remained inside the sample. If encoding is done without spatial selectivity, again the same integration as in Eq. (12) must be performed, and also in this case ϱ_{nmr} is identical for hyperpolarized and equilibrium polarized media.

2.4. Time-of-flight versus single-step detection

While the optimum sensitivity with remote detection is obtained if the volume of the void space inside the analyte, V_p, and the detection volume, V_d, are matched, a TOF experiment requires sacrificing some of the sensitivity by reducing V_d and applying multiple detection steps after each encoding step. This provides an encoded data set for each sampled time between encoding and detection. If, for example, an image is encoded, the fluid from different locations reaches the detector at different times – the farther it was encoded from the detector, the later it usually arrives there. A partial image is obtained for each TOF, corresponding to the fluid a certain time away from reaching the detector. Comparing images at different TOF allows one to follow the fluid as it crosses the sample. To avoid artifacts and to maintain good sensitivity in a TOF experiment, the time between subsequent detection pulses should correspond to the time it takes the fluid to flow through the detection volume. Let us assume that with TOF detection, τ_r is split into n detection steps, as shown in Fig. 2A. The acquisition time for each detection step shall be $t_t^{max} = (\tau_r - t_1^r)/n \approx \tau_r/n$. The index t denotes the respective parameters with TOF detection. The approximation assumes $t_1^r \ll \tau_r$. If $T_2^r > t_t^{max}$, the signal decay time with stroboscopic detection, T_2^t, is effectively determined by the time of the outflow of the fluid from the detection volume. Setting T_2^t to half of the time it takes the fluid to flow through the detection volume,

$$T_2^t = \frac{\tau_r}{2n}, \tag{13}$$

is a reasonable estimate. This allows one to calculate the relative sensitivity between one acquisition in a TOF experiment and single-step remote detection, where all the encoded fluid is detected in a single event, by using Eq. (6) with the respective parameters for the two experiments. The total time for each repetition is τ_r in both cases, therefore the relative duty cycle is T_2^t/T_2^r, and one obtains

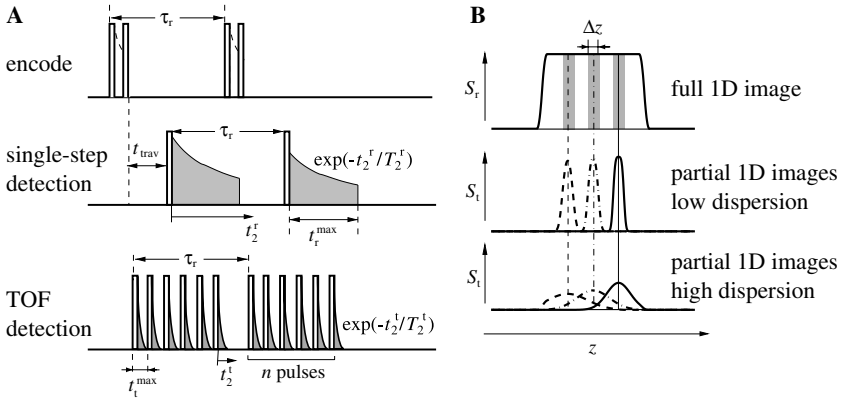

Fig. 2. Remote detection experiment with single-step and with TOF detection. (A) Timing of the experiments. The encoding sequence is independent of the detection method (upper). Single-step detection uses a single pulse, timed such that all of the encoded fluid is in the detection volume (middle). With TOF detection, a train of n pulses is used to stroboscopically resolve the TOF of the sensor fluid from the encoding location to the detector (lower). (B) Illustration of the signal in a single-step and a partial 1D image. (upper) With single-step detection or if all the partial images with TOF detection are added, the full image is obtained. The gray areas correspond to partial images if there were no dispersion at all. (middle) The part of the image acquired at a particular TOF has the same amplitude as the corresponding slice of the full image if the spatial dispersion width is lower than the resolution of the image, Δz. (lower) If the dispersion width is larger than Δz, the signal at each location gets spread across multiple TOF values, and each amplitude is significantly reduced. λ in Eq. (14) must be scaled accordingly.

$$\frac{\Psi_t}{\Psi_r} = \lambda\sqrt{\left[\frac{T_2^t}{T_2^r}\right]\left[1-\exp\left(-\frac{2t_r^{max}}{T_2^r}\right)\right]^{-1}} \approx \lambda\sqrt{\frac{T_2^t}{T_2^r}} = \lambda\sqrt{\frac{\tau_r}{2nT_2^r}}, \tag{14}$$

where λ is the relative sensitivity between the detectors with the small and the big detection volume. For the approximation, $t_r^{max} > T_2^r$ was assumed, and for the TOF experiment, $1-\exp(-2t_t^{max}/T_2^t) \approx 1$ was used. Eq. (14) gives an upper limit estimate of the sensitivity ratio of a partial to a single-step image. If spatial encoding is done in the flow direction of the sensor medium and the dispersion of the fluid between encoding location and detector is low, it is possible that the sinusoidal pattern of the longitudinal magnetization after the storage pulse is preserved during the flow. Partial images can then have almost the full local amplitude, and their sensitivity is given by Eq. (14). If the spatial dispersion of the fluid is larger than the image resolution, the signal of partial images is reduced, and Ψ_t/Ψ_r is scaled proportionally. This is illustrated in Fig. 2B.

To get the full image with TOF detection, all n partial images must be added up, which causes the noise to scale with $\sqrt{n}$. This degrades the sensitivity, Ψ_t^{full}, of the full image accordingly, and

$$\frac{\Psi_t^{full}}{\Psi_r} \approx \frac{\lambda}{n}\sqrt{\frac{\tau_r}{2T_2^r}}. \tag{15}$$

Therefore, if the coil-size dependence of λ is disregarded, the sensitivity to obtain the full image with TOF detection scales with $1/n$ compared to single-step detection.

2.5. Influence of the coil size

The above discussion does not take into account that a smaller detector can be made more sensitive than a large one. Detailed discussions can be found in the literature [17,18]. To give only a rough estimate for λ and also Λ if an inductive detector is used, we can use the SNR equation

$$\psi_{LCR} = K\eta M_0 V_c\sqrt{\frac{Q\omega_0}{V_c T\Delta f}} = \frac{Km_0}{2}\sqrt{\frac{Q\omega_0}{V_c T\Delta f}}, \tag{16}$$

where K is a numerical factor which depends on coil geometry, the noise figure of the preamplifier, and also takes into account various physical constants. M_0 is the nuclear magnetization, V_c is the volume of the coil, $\eta \approx V_d/2V_c$ is the filling factor of the sample in the detection coil, Q is the quality factor and ω_0 is the resonance frequency of the rf circuit, T is the temperature of the probe, and Δf is the detection bandwidth [17,19]. Δf in a pulsed NMR experiment is inversely proportional to T_2 and has already been included in Eqs. (7) and (10). $m_0 = M_0 V_d$ is the net magnetic moment of the spins inside the coil volume, which is transported without loss from the encoding to the detection location in an ideal remote experiment. λ can be estimated if we note that the only factors that change by scaling the coil are Q and V_c. In the ideal case, the small volume is contained n times in the big volume, $V_c^t/V_c^r = 1/n$, therefore

$$\lambda = \sqrt{\frac{Q_t/V_c^t}{Q_r/V_c^r}} = \sqrt{n\frac{Q_t}{Q_r}}, \tag{17}$$

where Q is typically lower for smaller coils [18], but as a very rough upper limit estimate, one gets back a factor of $\sqrt{n}$ in sensitivity by using a smaller coil in the TOF experiments. Therefore, partial images can be obtained with a minimum loss in sensitivity compared to a full image using a detector with a matched volume. If the spatial resolution in the flow direction is coarse enough that images of adjacent TOF values cover a distinct fraction of the sample volume, Ψ_t/Ψ_r may even be independent of n.

To experimentally determine the relative sensitivity between two coils, the principle of reciprocity, which states that the SNR is proportional to the B_1 field of a coil induced by a unit current at the sample location, can be very helpful. Since the duration of a 90° pulse, t_{90}, is inversely proportional to B_1, one can simply use

$$\Lambda = \frac{t_{90}^{\mathrm{d}}}{t_{90}^{\mathrm{r}}} = \sqrt{\frac{K_{\mathrm{r}} Q_{\mathrm{r}} \omega_0^{\mathrm{r}} / \tau_{\mathrm{r}} V_{\mathrm{c}}^{\mathrm{r}}}{K_{\mathrm{d}} Q_{\mathrm{d}} \omega_0^{\mathrm{d}} / \tau_{\mathrm{d}} V_{\mathrm{c}}^{\mathrm{d}}}}. \tag{18}$$

It was assumed that m_0 does not change between encoding and detection. The SNR in a remote experiment can be enhanced by optimizing $V_{\mathrm{c}}^{\mathrm{r}}$, Q_{r}, ω_0^{r}, τ_{r}, or the coil geometry (K_{r}). The flexibility is increased by considering the option to use alternative detectors. Magnetometers, for example, offer the possibility to measure the longitudinal magnetization, which can have a lifetime of tens of minutes in the case of a noble gas as sensor medium, even at low field [11]. Therefore, the time constant to measure one data point can be adjusted to the required sensitivity by changing the duration of the acquisition, which could be useful in experiments that inherently allow for very few encoding steps only.

2.6. Influence of multiplicative noise

Remote detection is affected by multiplicative noise (or t_1 noise) [4,20], caused by fluctuations of the signal-inducing quantity, for example, due to instabilities of the polarization and flow rate of the sensor medium or the spectrometer and its environment. A larger signal contributes a proportionately higher noise figure. This is a problem that is minor in a transiently detected dimension, where this kind of noise mainly appears as a collective fluctuation of the phase and amplitude of all the peaks in a spectrum. However, in experiments with point-by-point detection, the correlation of the noise between adjacent data points is lost, resulting in a frequency-independent noise figure (white noise). In addition, the noise across the entire spectrum will be determined by the most intense peaks. Thus, less intense peaks are doomed to compete with the large noise figure from the intense peaks, sometimes rendering the smaller peaks undetectable. This multiplicative noise poses an upper limit on the SNR that can be obtained. If this limit is reached, increasing the signal does not improve the sensitivity anymore, as the noise increases accordingly. Because multiplicative noise is proportional to the signal, it is a bigger problem with Boltzmann polarized fluids, where the signal relaxes towards a maximum, than with hyperpolarized fluids, where this signal relaxes towards a very small or even undetectable value.

A simplified analytical treatment of multiplicative noise can be done by calculating the noise variance σ_S^2 by doing an expansion of the signal about its theoretical value. Let us consider a simple TOF experiment where the encoding step consists of a 180° pulse to invert the spin magnetization of the fluid. This magnetization is then measured as a function of the time t_{TOF} as it arrives at the detector. We can model the signal in a very general way as

$$S(t_{\mathrm{TOF}}) = \zeta(t_{\mathrm{TOF}}) S_0, \tag{19}$$

where $\zeta(t_{\mathrm{TOF}})$ is a function of the sample geometry as well as the fluid properties and flow rate. S_0 is the signal one obtains from unencoded fluid. In experiments with remote detection, the flow rate is always a potential source of multiplicative noise. If we assume a sample through which the flow velocity v is uniform, we can write

$$\sigma_S^2 = \left(\frac{\partial S}{\partial v}\right)^2 \sigma_v^2, \tag{20}$$

with the variance σ_v^2 of the flow velocity. If we relate this flow velocity to t_{TOF} through $v = z/t_{\mathrm{TOF}}$, with the flow distance z between encoding and detection, we can use $\mathrm{d}v/\mathrm{d}t_{\mathrm{TOF}} = -z/t_{\mathrm{TOF}}^2$ to obtain

$$\sigma_S = \left|\frac{\mathrm{d}S(t_{\mathrm{TOF}})}{\mathrm{d}t_{\mathrm{TOF}}} \frac{t_{\mathrm{TOF}}^2}{z}\right| \sigma_v = S_0 t_{\mathrm{TOF}} \left|\frac{\mathrm{d}\zeta(t_{\mathrm{TOF}})}{\mathrm{d}t_{\mathrm{TOF}}}\right| \frac{\sigma_v}{v}. \tag{21}$$

This states that σ_S is proportional to the rate of change of $S(t_{\mathrm{TOF}})$ and increases linearly with t_{TOF} as long as changes of v are slow on the time scale of t_{TOF}. $(\sigma_v/v)^2$ is the variance normalized to v, which is often a better measure for fluctuations of v than σ_v, as σ_v commonly increases synchronously with v. Experimentally, $\sigma_S(t_{\mathrm{TOF}})$ can be obtained by repeating the same experiment a large number of times and then calculating

$$\sigma_S(t_{\mathrm{TOF}}) = \sqrt{\langle |S(t_{\mathrm{TOF}}) - \langle S(t_{\mathrm{TOF}})\rangle|^2\rangle}. \tag{22}$$

The result of such an experiment is shown in Fig. 3. Fig. 3A shows $S(t_{\mathrm{TOF}})$ in an experiment with encoding and detection both done at high field in the sweet spot of a 7 T magnet. Forty detection pulses were applied, spaced by 15 ms, to record the dispersion curve of a gas as it flows from the encoding volume, which is a glass cylinder with a volume of about 10 ml, to the detector, with a volume of about 0.7 ml. Hyperpolarized ^{129}Xe gas was used as the spin sensor. Fig. 3B shows $\sigma_S(t_{\mathrm{TOF}})/S_0$. One can see the large increase of the noise at the leading and tailing edge of the TOF curve. In the center, where $\mathrm{d}S/\mathrm{d}t_{\mathrm{TOF}} = 0$, the noise level drops almost to the value of the unencoded gas. Furthermore, one can also see that noise increases with larger t_{TOF}. For an optimum sensitivity in an experiment without TOF detection, this suggests that either the detection volume should be smaller than the encoding volume and the detection step carefully timed to the instant when the amount of encoded fluid in the detection volume is at its maximum, or that the detection volume should be bigger than the encoded volume so that all the encoded gas can be collected. The best solution is of course to optimize the flow rate stability. In this experiment, the tubing on the outlet side of the detector was vented to air without an additional valve. Controlling the flow rate with valves at the inlet and the outlet side of the experiment usually helps to get more stable flow conditions.

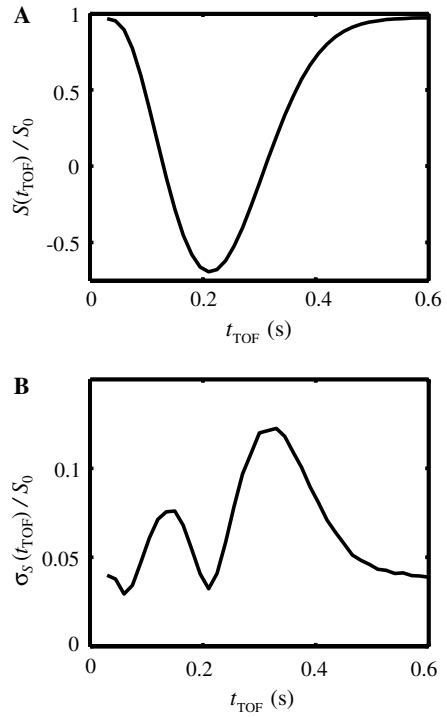

Fig. 3. Experiment to measure the impact of multiplicative noise with remote detection. The magnetization of hyperpolarized ^{129}Xe in a mixture of Xe/N_2/He = 1:10:89 was inverted with a hard 180° pulse and then measured with a train of 40 detection pulses spaced by 15 ms, using a second, smaller coil on the outlet side of the encoding volume. One hundred identical experiments were recorded, and the data was used to calculate the reproducibility of the signals. (A) Dispersion curve that shows how the encoded gas arrives at the detector. Maximum signal is obtained with unencoded gas. The signal drops when encoded gas arrives in the detector, and then rises again to its steady-state value. (B) Noise level relative to the signal. The noise is maximum in the slopes of the dispersion curve. Since the additive noise level was only about 0.5% of the signal, the minimum noise level is still dominated by multiplicative noise. But the origin there is more likely due mechanical vibrations and fluctuations of the static magnetic field.

3. Examples and practical considerations

To illustrate the benefits and limitations of remote detection, the sensitivity of three experiments with different objectives is compared with direct detection. The first experiment uses encoding at a low magnetic field and detection at high field, the second describes the sensitivity of NMR and MRI in a microfluidic device, with encoding done with a coil surrounding the whole device, and the third considers encoding in an environment with strong susceptibility gradients. Note that actual values for the sensitivity depend strongly on the specific implementation of an experiment, therefore these numbers should be understood neither as best nor worst case scenario, but as an illustration of the potential of remote detection in different circumstances.

In [1], an MRI experiment was presented with signal encoding at a $B_0^d = 4\,\mathrm{mT}$ and detection at $B_0^r = 4.2\,\mathrm{T}$. The sample whose void space was imaged did not show any significant susceptibility broadening, therefore the sensitivity advantage was primarily due to a higher sensitivity of the detection coil. The coil used for encoding was by no means sensitive enough for detection, even using hyperpolarized ^{129}Xe. This caused additional problems as shimming of the encoding volume was extremely tedious without the ability to directly measure a signal, therefore annihilating the advantage of a smaller linewidth one would have at lower fields for a given relative field homogeneity [21]. In this case, it is reasonable to state that the relative sensitivity between remote and direct detection is on the order of Λ. While the high-field probe had a $Q_r \approx 100$, the low-field circuit had a very low Q_d of only about 5 due to the high resistance of the coil. The resonance frequency is proportional to the magnetic field, therefore $\omega_0^r/\omega_0^d \approx 1000$, and the overall sensitivity gain can be, according to Eq. (18), estimated to about two orders of magnitude if we assume $K_r \approx K_d$, $\tau_r \approx \tau_d$, and $V_c^r \approx V_c^d$. An additional factor not considered in this treatment is that if detection were done at the encoding frequency of about 50 kHz, additional shielding would be necessary to reduce external noise. This experiment was done in stopped-flow mode, using a closed loop for the gas mixture. The stopped-flow approach requires waiting after closing the valve until the fluid has settled in the encoding volume. This is, however, not specific to remote detection, but would also be necessary in an experiment with direct detection, therefore does not contribute unfavorably to the performance of remote detection. More importantly, this experiment was plagued considerably by multiplicative noise. While each data point could be recorded with an SNR of about 10, as can be seen from the travel time data shown in [1], the overall sensitivity of the image was considerably lower because the flow rate was not stable enough. Additionally in this setup, the distance between the encoding and the detection volume was about 5 m, while in the experiments with encoding and detection at high field, this distance was only a few centimeters, with a correspondingly shorter t_{trav}. In the following experiments, multiplicative noise was reduced significantly by using an open flow circuit for the gas, which was vented to air through a valve at the outlet side of the detector. This approach did not require a pump since the necessary pressure to drive the flow was provided from the gas bottle where the gas mixture was stored. Furthermore, these experiments were done in continuous flow mode, which has a lower susceptibility to multiplicative noise than stopped-flow mode.

Gas flow profiling in a microfluidic device is another example where remote detection was used [7]. In this case, the primary challenge was that the size of the microfluidic device was on the order of centimeters, while the fluid channels had volumes on the order of one microliter or below. Using a large coil that fits the whole chip would require a diameter on the order of 20 mm and therefore have a very low filling factor. With direct detection, the only option to get a high enough sensitivity would be to design a coil specifically for a certain device, like a small

surface coil in the direct vicinity of the flow channels [22]. In [7], the microfluidic device was placed in a microimaging probe with a sample bore of 30 mm. Its coil had a volume of about 45 ml, while the fluid volume was less than 1 μl, therefore the filling factor was only about $\eta = 10^{-5}$. By using a microsolenoid coil with a matched volume, the sensitivity can be improved by about two orders of magnitude, which was also found experimentally by taking the ratio of the 90° times of the detection and the encoding coil at a given rf power level [23].

The last example discusses a gas flow study through a porous Bentheimer sandstone that showed significant susceptibility broadening of the spectrum [5]. The rock was cylindrically shaped, with a diameter of 20 mm and a height of 38 mm. Its porosity was 22.5%, with pore sizes of about 100 μm. The signal dephasing time at a field of 7 T, again using hyperpolarized ^{129}Xe as the NMR-active component of the gas, was about $T_2^{\mathrm{d}} = 1$ ms. T_1^{d} of ^{129}Xe depended on the pressure and was between 5 s and 10 s inside the rock, which is well above the typical time of 1 s that it took the gas to flow through the rock. Using Eqs. (10) and (18), one can estimate the potential of an experiment with remote detection to optimizes the sensitivity. The detection coil could be made about a factor 4 smaller than the encoding coil, corresponding to the inverse of the sample porosity. Assuming identical values for all the other parameters with an impact on Λ, this would only amount to a factor 2 in sensitivity. However, if we consider continuous flow and use the—somewhat optimistic—assumption of $T_2^{\mathrm{r}} = \tau_{\mathrm{r}}/2 = 500$ ms with the repetition time τ_{r} set to the time it takes to replace all the gas in the rock, analogous to the discussion of TOF sensitivity, we get $T_2^{\mathrm{r}}/T_2^{\mathrm{d}} \approx 500$. This would amount to about a factor 30 in sensitivity enhancement with remote detection. In this case, it was assumed that the volume of the detection coil was matched to the volume of the fluid inside the rock. In these experiments, the time for the encoding sequence could be reduced to about 200 μs, which was considerably shorter than T_2^{d}. This shows that it would be possible with this approach to study samples with even bigger susceptibility gradients. However, some of these samples may have a high density of paramagnetic centers on the surface of the pores, causing a much shorter T_1^{d}. This effect may be compensated to a certain degree by using a smaller sample with a shorter τ_{i}, but it would eventually limit the use of remote detection.

As the experiments presented in [5] were done with the objective to study flow in a TOF experiment, the volume of the detection coil was smaller than the volume of the encoded fluid. Detection was done with a 10 mm diameter saddle coil. The gas volume inside the detection coil was set to about 1/15 of the total pore volume. The detection coil, though, was only about a factor 2.3 smaller than the total pore volume. This caused some sensitivity loss, but allowed the use of a thicker-walled tubing through the coil to stabilize the whole setup and minimize t_1 noise. Furthermore, the inner diameter of the tubing could be varied, therefore it was not necessary to design the detection coil specifically for one particular application. The outflow of encoded gas was recorded with typically $n = 25$ detection steps and 50 ms repetition time between subsequent detection pulses. Using Eq. (13), the sensitivity of the partial images compared to a full image with single-step detection can be approximated as $\Psi_{\mathrm{t}}/\Psi_{\mathrm{r}} \approx \sqrt{2.3}\sqrt{25^{-1}} \approx 0.3$. And compared to an image with direct detection, each remotely detected partial image was recorded with a sensitivity gain of about one order of magnitude.

4. Conclusion

It was shown that remote detection offers a valuable alternative for sensitivity enhancements of certain NMR experiments, mainly with samples that cannot be tailored to fit the restrictive requirements of high-resolution setups. Porous media imaging experiments have especially large potential for sensitivity improvements, while spectroscopic experiments are more limited and typically require a detector that is at least an order of magnitude more sensitive to see a noticeable sensitivity improvement. On the downside, encoding with remote detection is done point-by-point, therefore if enough sensitivity is available with direct detection, this approach is usually faster and opens more flexibility for trading sensitivity for resolution. Also, not all porous materials and fluids are suitable for remote detection. If the permeability of a material is too low or if the longitudinal relaxation time of the fluid is too short, fast enough flow may not be achievable to allow any encoded spin magnetization to survive the transfer to the detector.

TOF experiments, if set up properly, do not suffer a large sensitivity penalty by splitting the detection into multiple steps, while gaining an additional transient dimension that provides information about fluid flow and dispersion without increasing the total experiment time. If dispersion is low between encoding and detection such that a tight correlation between the encoding position and the arrival time at the detector exists, experiment time may be reduced by spatially encoding multiple data points at different locations in the sample [24] and separating them by their time of arrival at the detector, therefore providing a possibility to somewhat loosen the strict statement that only one data point can be encoded at a time.

Acknowledgments

We are grateful to Alex Pines for his encouragement, support, and critical validation of this work. We thank Song-I Han, Christian Hilty, and Elad Harel for helpful discussions. This work was supported by the Director, Office of Science, Office of Basic Energy Sciences, Materials Sciences and Nuclear Science Divisions, of the U.S. Department of Energy under contract DE-AC03-76SF00098. J.G. gratefully acknowledges the Swiss National Science Foundation for support through a postdoctoral fellowship.

References

[1] A.J. Moulé, M.M. Spence, S. Han, J.A. Seeley, K.L. Pierce, S.K. Saxena, A. Pines, Amplification of xenon NMR and MRI by remote detection, Proc. Natl. Acad. Sci. USA 100 (2003) 9122–9127.

[2] J.A. Seeley, S. Han, A. Pines, Remotely detected high-field MRI of porous samples, J. Magn. Reson. 167 (2004) 282–290.

[3] T.G. Walker, W. Happer, Spin-exchange optical pumping of noble-gas nuclei, Rev. Mod. Phys. 69 (1997) 629–642.

[4] J. Granwehr, J.T. Urban, A.H. Trabesinger, A. Pines, NMR detection using laser-polarized xenon as a dipolar sensor, J. Magn. Reson. 176 (2005) 125–139.

[5] J. Granwehr, E. Harel, S. Han, S. Garcia, A. Pines, P.N. Sen, Y.-Q. Song, Time-of-flight flow imaging using NMR remote detection, Phys. Rev. Lett. 95 (2005) 075503.

[6] A. Abragam, Principles of Nuclear Magnetism, Oxford University Press, Oxford, 1961.

[7] C. Hilty, E.E. McDonnell, J. Granwehr, K.L. Pierce, S. Han, A. Pines, Microfluidic gas-flow profiling using remote-detection NMR, Proc. Natl. Acad. Sci. USA 102 (2005) 14960–14963.

[8] E. Fukushima, Nuclear magnetic resonance as a tool to study flow, Annu. Rev. Fluid Mech. 31 (1999) 95–123.

[9] J.D. Seymour, P.T. Callaghan, Generalized approach to NMR analysis of flow and dispersion in porous media, AIChE J. 43 (1997) 2096–2111.

[10] Y.S. Greenberg, Application of superconducting quantum interference devices to nuclear magnetic resonance, Rev. Mod. Phys. 70 (1998) 175–222.

[11] V.V. Yashchuk, J. Granwehr, D.F. Kimball, S.M. Rochester, A.H. Trabesinger, J.T. Urban, D. Budker, A. Pines, Atomic magnetometry for detection of nuclear magnetization, Phys. Rev. Lett. 93 (2004) 160801.

[12] D. Raftery, H.W. Long, D. Shykind, P.J. Grandinetti, A. Pines, Multiple-pulse nuclear magnetic resonance of optically pumped xenon in a low magnetic field, Phys. Rev. A 50 (1994) 567–574.

[13] R.R. Ernst, G. Bodenhausen, A. Wokaun, Principles of Nuclear Magnetic Resonance in One and Two Dimensions, Clarendon Press, Oxford, 1987.

[14] M.H. Levitt, G. Bodenhausen, R.R. Ernst, Sensitivity of Two-Dimensional Spectra, J. Magn. Reson. 58 (1984) 462–472.

[15] N. Murali, A. Kumar, Multiple-quantum artifacts in single-quantum two-dimensional correlated NMR spectra of strongly coupled spins, Chem. Phys. Lett. 128 (1986) 58–61.

[16] R. Wang, R.W. Mair, M.S. Rosen, D.G. Cory, R.L. Walsworth, Simultaneous measurement of rock permeability and effective porosity using laser-polarized noble gas NMR, Phys. Rev. E 70 (2004) 026312.

[17] D.I. Hoult, R.E. Richards, The signal-to-noise ratio of the nuclear magnetic resonance experiment, J. Magn. Reson. 24 (1976) 71–85.

[18] D.L. Olson, T.L. Peck, A.G. Webb, R.L. Magin, J.V. Sweedler, High-resolution microcoil ^{1}H NMR for mass-limited, nanoliter-volume samples, Science 270 (1995) 1967–1970.

[19] R. Freeman, A Handbook of Nuclear Magnetic Resonance, second ed., Longman, Singapore, 1997.

[20] A.F. Mehlkopf, D. Korbee, T.A. Tiggelman, R. Freeman, Sources of t_1 noise in two-dimensional NMR, J. Magn. Reson. 58 (1984) 315–323.

[21] A.H. Trabesinger, R. McDermott, S.K. Lee, M. Mück, J. Clarke, A. Pines, SQUID-detected liquid state NMR in microtesla fields, J. Phys. Chem. A 108 (2004) 957–963.

[22] J.D. Trumbull, I.K. Glasgow, D.J. Beebe, R.L. Magin, Integrating microfabricated fluidic systems and NMR spectroscopy, IEEE Trans. Biomed. Eng. 47 (2000) 3–7.

[23] E.E. McDonnell, S. Han, C. Hilty, K.L. Pierce, A. Pines, NMR analysis on microfluidic devices by remote detection, Anal. Chem. 77 (2005) 8109–8114.

[24] L. Frydman, T. Scherf, A. Lupulescu, The acquisition of multidimensional NMR spectra within a single scan, Proc. Natl. Acad. Sci. USA 99 (2002) 15858–15862.